Supplementary Data

Alteration of myocardial structure and function in RAF1associated Noonan syndrome: Insights from cardiac disease modeling based on patient-derived iPSCs

Saeideh Nakhaei-Rad1,16,(†) , Farhad Bazgir1,(†) , Julia Dahlmann2,3,16,‡ , Alexandra Viktoria Busley4,5,6,‡ , Marcel Buchholzer1,16,‡ , Fereshteh Haghighi1,3,5,‡ , Anne Schänzer7 , Andreas Hahn8 , Sebastian Kötter9 , Denny Schanze2 , Ruchika Anand10 , Florian Funk11 , Andrea Borchardt10 , Annette Vera Kronenbitter11 , Jürgen Scheller1 , Roland P. Piekorz1 , Andreas S. Reichert10 , Marianne Volleth2 , Matthew J. Wolf12 , Ion Cristian Cirstea13 , Bruce D. Gelb14 , Marco Tartaglia15 , Joachim Schmitt11 , Martina Krüger9 , Ingo Kutschka3,5 , Lukas Cyganek4,5,6 , Martin Zenker2,* , George Kensah3,5,* , Mohammad R. Ahmadian1,*

1 Institute of Biochemistry and Molecular Biology II, Medical Faculty and University Hospital Düsseldorf, Heinrich Heine University Düsseldorf, Düsseldorf, Germany
(†) These authors contributed equally: Saeideh Nakhaei-Rad, Farhad Bazgir
‡ These authors contributed equally: Julia Dahlmann, Alexandra Viktoria Busley, Marcel Buchholzer, Fereshteh Haghighi
*Corresponding authors: reza.ahmadian@uni-duesseldorf.de; george.kensah@med.uni-goettingen.de; martin.zenker@med.ovgu.de.

Abstract
Noonan syndrome (NS), the most common among the RASopathies, is caused by germline variants in genes encoding components of the RAS-MAPK pathway. Distinct variants, including the recurrent Ser257Leu substitution in RAF1, are associated with severe hypertrophic cardiomyopathy (HCM). Here, we investigated the elusive mechanistic link between NS-associated RAF1S257L and HCM using three-dimensional cardiac bodies and bioartificial cardiac tissues generated from patient-derived induced pluripotent stem cells (iPSCs) harboring the pathogenic RAF1 c.770C>T missense change. We characterize the molecular, structural and functional consequences of aberrant RAF1 –associated signaling on the cardiac models. Ultrastructural assessment of the sarcomere revealed a shortening of the I-bands along the Z disc area in both iPSC-derived RAF1S257L cardiomyocytes, and myocardial tissue biopsies. The disease phenotype was partly reverted by using both MEK inhibition, and a gene-corrected isogenic RAF1L257S cell line. Collectively, our findings uncovered a direct link between a RASopathy gene variant and the abnormal sarcomere structure resulting in a cardiac dysfunction that remarkably recapitulates the human disease. These insights represent a basis to develop future targeted therapeutic approaches.

Keywords: Cardiac bodies, hypertrophic cardiomyopathy, iPSC, MAPK pathway, Noonan syndrome, RAF kinase, RASopathy, sarcomere

Table S1. The list of primers used in this study.

Name	Sequence	Accession number
Actinin alpha 1 (ACTN1)	CCCGAGCTGATTGACTACGG	NM_001130005.1
	GCAGTTCCAACGATGTCTTCG	
Alpha fetoprotein (AFP)	GAATGCTGCAAACTGACCACGCTGGAAC	NM_001354717.1
	TGGCATTCAAGAGGGTTTTCAGTCTGGA	
Actin beta (ACTB)	AGCCTCGCCTTTGCCGA	NM_001101.5
	CTGGTGCCTGGGGCG	
Calcium voltage-gated channel subunit alpha1 C (CACNA1C)	TGATTCCAACGCCACCAATTC	NM_199460.3
	GAGGAGTCCATAGGCGATTACT	
Calcium voltage-gated channel subunit alpha1 D (CACNA1D)	CGCGAACGAGGCAAACTATG	NM_001128840.2
	TTGGAGCTATTCGGCTGAGAA	
Troponin T2, cardiac type (TNNT2)	GGAGGAGTCCAAACCAAAGCC	NM_001001430
	TCAAAGTCCACTCTCTCTCCATC	
Forkhead box A2 (FOXA2)	TGGGAGCGGTGAAGATGGAAGGGCAC	NM_021784.4
	TCATGCCAGCGCCCACGTACGACGAC	
Hypoxanthine phosphoribosyl-transferase 1 (HPRT1)	CCTGGCGTCGTGATTAGTGAT	NM_000194.2
	AGACGTTCAGTCCTGTCCATAAT	
Kruppel like factor 4 (KLF4)	CAGCTTCACCTATCCGATCCG	NM_001314052.1
	GACTCCCTGCCATAGAGGAGG	
Myosin heavy chain 6 (MYH6)	GCCCTTTGACATTCGCACTG	NM_002471.3
	GGTTTCAGCAATGACCTTGCC	
Myosin heavy chain 6 (MYH7)	ACTGCCGAGACCGAGTATG	NM_000257.3
	GCGATCCTTGAGGTTGTAGAGC	
Myosin heavy chain 7B (MYH7B)	AGTGGCAATAAAAGGGGTAGC	NM_020884.4
	CCAAGTTCACTCACATCCATCA	
Myosin light chain (MYL2)	TTGGGCGAGTGAACGTGAAAA	NM_000432.3
	CCGAACGTAATCAGCCTTCAG	
Myosin light chain 7 (MYL7)	CATCAACTTCACCGTCTTCC	NM_021223.2
	GAAGCTGCTTGAACTCATCC	
Nanog homeobox (NANOG)	CCCCAGCCTTTACTCTTCCTA	NM_024865.3
	CCAGGTTGAATTGTTCCAGGTC	
Natriuretic peptide A (NPPA)	CAACGCAGACCTGATGGATTT	NM_006172.3
	AGCCCCCGCTTCTTCATTC	
Natriuretic peptide B (NPPB)	TCCTGCTCCTGCTCTTCTTG	NM_002521.2
	TCCTGTAACCCGGACGTTTC	
NK2 homeobox 5 (NKX2-5)	CCAGCCCTGCTCTCACG	NM_004387.4
	GCCCAGCGTAGGCCTCT	
POU class 5 homeobox 1 (POU5F1)/OCT4	CTGGGTTGATCCTCGGACCT	NM_002701.5
	CACAGAACTCATACGGCGGG	
Phospholamban (PLN)/PLB	ACCTCACTCGCTCAGCTATAA	NM_002667.4
	CATCACGATGATACAGATCAGCA	
Ryanodine receptor 2 (RYR2)	GGCAGCCCAAGGGTATCTC	NM_001035.2
	ACACAGCGCCACCTTCATAAT	
ATPase sarcoplasmic/endoplasmic reticulum Ca^{2+} transporting 2 (ATP2A2)/SERCA2	CATCAAGCACACTGATCCCGT	NM_001681.3
	CCACTCCCATAGCTTTCCCAG	

SRY-box 2 (SOX2)	GCCGAGTGGAAACTTTTGTCG	NM_003106.3
	GGCAGCGTGTACTTATCCTTCT	
SRY-box 17 (SOX17)	CGCTTTCATGGTGTGGGCTAAGGACG	NM_022454.4
	TAGTTGGGGTGGTCCTGCATGTGCTG	
Titin (TTN)	CCCCATCGCCCATAAGACAC	NM_133378
	CCACGTAGCCCTCTTGCTTC	
Troponin C1, slow skeletal and cardiac type (TNNC1)	TGGTTCGGTGCATGAAGGAC	NM_003280.2
	GTCGATGTAGCCATCAGCATTT	
Troponin I3, cardiac type (TNNI3)	AGAAGGAGGACACCGAGAAG	NM_000363.4
	GGAAGGCTCAGCTCTCAAAC	
Tubulin beta 3 class III (TUBB3)	ATGAGGGAGATCGTGCACAT	NM_006086.4
	GCCCCTGAGCGGACACTGT	
Skeletal muscle (ACTA1)/α-SK (ACTA1)	TGCCAACAACGTCATGTCG	NM_001100.3
	CAGCGCGGTGATCTCTTTCT	
Smooth muscle (ACTA2)/α-SMA	AAAAGACAGCTACGTGGGTGA	NM_001613
	GCCATGTTCTATCGGGTACTTC	
Titin (N2B isoform)	GGCCGAGAAATTTATGAGAGTGAC	NM_003319.4
	CGCTTTTCAGAACAACTTCTTCCT	
Titin (N2BA isoform)	CCAGCAACCAAGAAAGCTGCG	NM_001256850.1
	CCCAGAATCAGTTTTTGTGGTGTC	

Table S2. Reagents used in this study.

REAGENT	SOURCE	IDENTIFIER
Antibodies		
anti-OCT3/4	Santa Cruz	#sc-5279
anti-cardiac troponin t	Thermo Scientific	#MA5-12960
anti-Tra-1-60	Abcam	#ab16288
anti-Myosin light chain 2 V	Synaptic Systems	#310111
anti-SSEA4	DSHB	#MC-813-70
anti- γ -tubulin	Sigma-Aldrich	#T5326
anti-phospho-ERK1/2 T202/T204	Cell Signaling	#9106
Anti-phospho-AKT S473	Cell Signaling	#4060
Anti-phospho-AKT T308	Cell Signaling	#2965
anti-phospho-YAP Ser127	Cell Signaling	#4911
anti-YAP	Cell Signaling	#4912
anti-JNK	Cell Signaling	#9252
anti-phospho-JNK Thr183/Tyr185	Cell Signaling	#9251
anti-S6K	Cell Signaling	#2708
anti-phospho-S6K Thr389	Cell Signaling	#9205
anti-phospho-p38 Thr180/Tyr182	Cell Signaling	#9211
anti-p38	Cell Signaling	#8690
anti-alpha-actinin	Sigma-Aldrich	#A7811
anti-ATP2A2/SERCA2	Cell Signaling	#4388
anti-RAF1	Abcam	#AB181115
anti-phospho-RAF1 S259	Abcam	#ab173539
anti-TUBB3	Thermo Scientific	#MA1-118
anti-Nkx2.5	Santa Cruz	#sc-14033
anti-Sox17	R&D Systems	#AF1924
anti-desmin	Agilent Technologies	#M076029-2
anti-troponin I	Abcam	#Ab47003
anti-SMA Clone 1A4	DAKO	#M0851
Custom made α-titin PEVK raised against PEVK S11878 (CEVVLKSVLRKR) and PEVK S12022 (LRPGSGGEKPP) (*Kötter, Sebastian, et al. Circulation research, 2016*)	Eurogentec	N/A
Anti-rabbit IgG Alexa Fluor 488 Conjugate	Cell Signaling	#4412
Anti-mouse IgG Alexa Fluor 555 Conjugate	Cell Signaling	#4409
Anti-mouse IgG Alexa Fluor 488 conjugated	Cell Signaling	#4408
IRDye® 800CW Donkey anti-Rabbit IgG	LI-COR Biosciences	#926-32213
IRDye® 800CW Donkey anti-Mouse IgG	LI-COR Biosciences	#926-32212
Alexa488-conjugated goat anti-rabbit IgG	Thermo Scientific	#A11034
Alexa546-conjugated goat anti-mouse IgG	Thermo Scientific	#A4671
Alexa488-conjugated goat anti-mouse IgG	Thermo Scientific	#A11029
Chemicals, peptides, and recombinant proteins		
B-mercaptethanol	Sigma-Aldrich	#M-3148
basic Fibroblast Growth Factor (bFGF)	Peprotech	#100-18B
ROCK-Inhibitor Y27632	Selleckchem	#S1049
CHIR99021	Selleckchem	#S1263
IWR-1	Sigma-Aldrich	#I0161
RPMI 1640 Medium, no glucose	Thermo Scientific	#11879-020
human Albumin	Sigma-Aldrich	#A0237
Sodium DL-Lactat	Sigma-Aldrich	#L4263
L-Ascorbic acid-2-Phosphate	Sigma-Aldrich	#A8960
DMEM / F12 + Glutamax	Thermo Scientific	#31331-028
Knockout Serum Replacement (KO-SR)	Thermo Scientific	#10828028

MEM Non-Essential Amino Acids	Thermo Scientific	#11140-035
RPMI 1640 Medium	Thermo Scientific	#21875-034
B-27™ Supplement, minus insulin	Thermo Scientific	#A1895601
B-27™ Supplement	Thermo Scientific	#17504044
Geltrex Membrane Matrix	Thermo Scientific	#A1413201
Gelatine from porcine skin	Sigma-Aldrich	#G2500
Accutase™ Cell Dissociation Reagent	Thermo Scientific	#A1110501
Collagenase, Type IV	Thermo Scientific	#17104019
Agarose NEEO Ultra-Quality	CARL ROTH	#2267.4
Hydrosil A and Hydrosil B	SILADENT	#101301
AggreWell™400	STEMCELL Technologies	#27840
Versene Solution	Thermo Scientific	15040066
TrypLE™ Select Enzyme	Thermo Scientific	A1285901
DMSO (dimethyl sulfoxide)	Sigma-Aldrich	#D2650
Fetal Bovine Serum	Thermo Scientific	26140079
L-Glutamine	Thermo Scientific	25030149
KaryoMAX Colcemid	Thermo Scientific	15212012
Trypsin/EDTA	Biochrom	L 2143
TRIzol™	Thermo Scientific	15596026
SYBR™ Green	Applied Biosystems	#4309155
Formaldehyde 4%	Carl Roth	#P087.1
EDTA-free protease inhibitor	Sigma-Aldrich	11873580001
Phosphate buffered saline with 5% non-fat milk	Merck	#P4739
Intercept® (TBS) Blocking Buffer	LI-COR	927-60001
ProLong™ Gold Antifade Mountant	Thermo Scientific	P10144
Tissue-Tek® O.C.T. Compound	Sakura Finetek	#4583

Cell Lines

HFF-1	ATCC	SCRC-1041

Recombinant DNA

pCE-hSK	Addgene	#41814
pCE-hOct3/4	Addgene	#41813
pCE-hUL	Addgene	#41855
pCE-mp53DD	Addgene	#41856
pCXB-EBNA1	Addgene	#41857

Oligonucleotides

For primers, please see Table S1

Software

FlowJo	Treestar, Ashland, OR	https://www.flowjo.com/
IKAROS	MetaSystems (Altlußheim, Germany)	https://metasystems-international.com/de/products/ikaros
Image Studio 5.2	LI-COR	https://www.licor.com/bio/image-studio-lite
ZEN 3.2 (blue edition)	Carl Zeiss AG	
IonWizard 6.4	Ion Optix Corp	http://www.ionoptix.com/
Prism 6	GraphPad software	https://www.graphpad.com/scientific-software/prism/

Critical Commercial Assays

DNA-free™ DNA Removal Kit	Invitrogen	AM1906
GoScript™ cDNA Synthesis Kit	Promega	A5003

Quick Start™ Bradford Protein Assay	Bio-Rad	5000201
Trichrome II Blue staining kit	Roche	#860-013
Other		
6-Well-Plate	Thermo Scientific	140675
T-25 Tissue Culture Flasks	TPP Techno Plastic	90026
T-175 Filter Cap Flasks	CELLSTAR	GR661175
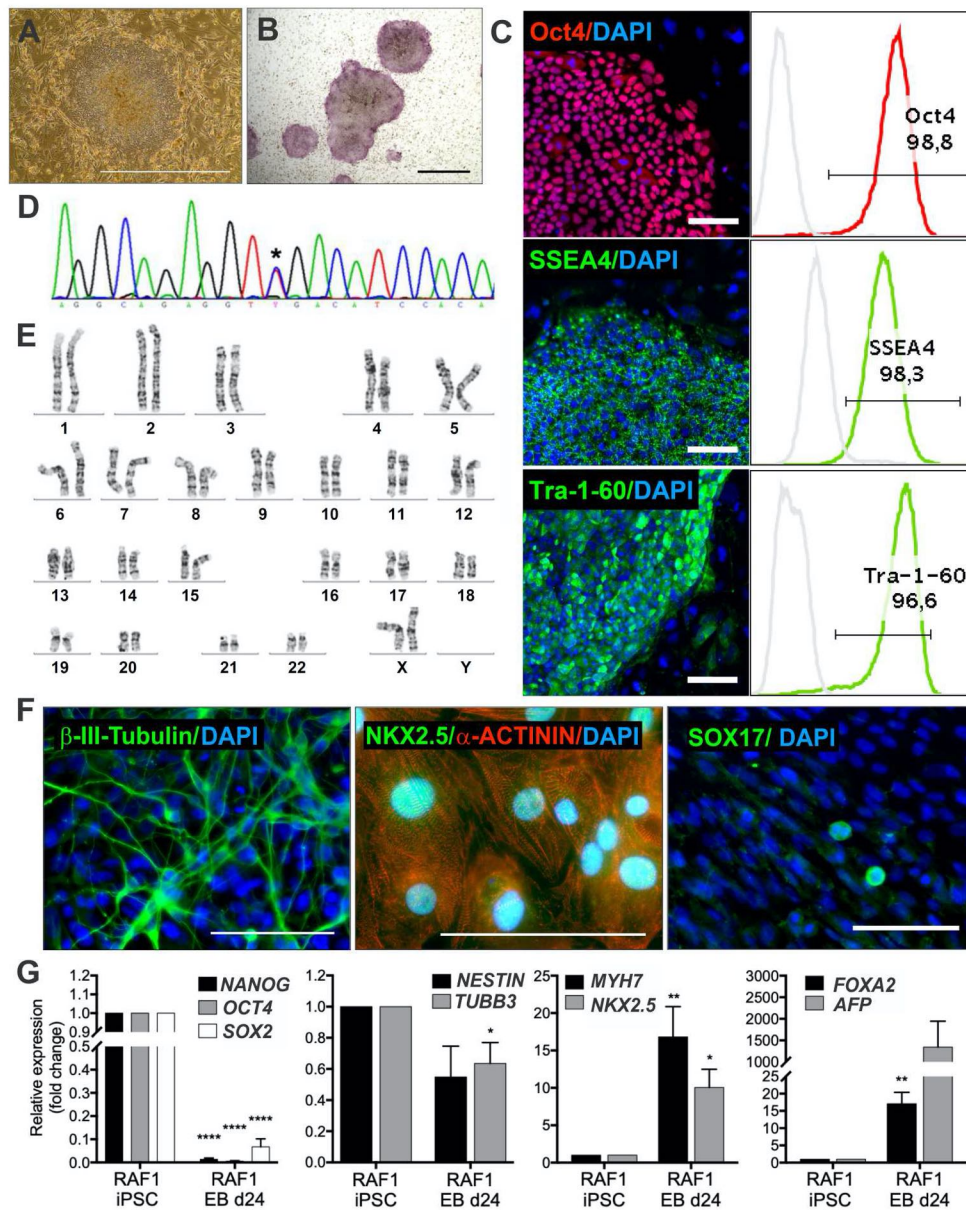
Figure S1. Characterization of RAF1^{S257L} iPSC line 1 (7B10) from first patient.

A) Typical iPSC colonies on mitotically inactivated murine feeder cells. Scale bar, 1000 µm.

B) Alkaline phosphatase-positive colonies. Scale bar, 1000 µm.

C) Expression of pluripotency markers OCT4, SSEA4, and TRA-1-60 as detected by immunofluorescence staining and flow cytometry. Scale bar, 100 µm. Isotype controls of flow cytometry histograms depicted in light gray.

D) Sanger sequencing confirmed the heterozygous *RAF1 c.770C>T* variant in iPSCs (asterisk).

E) Normal diploid karyotypes in iPSCs at passage 8 after reprogramming.

F) Trilineage differentiation of patient derived iPSCs. Expression of ectodermal (beta-III-Tubulin), mesodermal (NKX2.5 and sarcomeric alpha-actinin), and endodermal (SOX17) markers was detected. Scale bars, 100 µm.

G) Relative gene expression of pluripotency (*NANOG*, *OCT4*, *SOX2*) and differentiation markers (*NESTIN*, *TUBB3*, *MYH7*, *NKX2.5*, *FOXA2*, *AFP*) of differentiated embryoid bodies on d24 of differentiation relative to undifferentiated iPSCs normalized by beta-ACTIN expression. Bar graphs represent mean of three independent samples +/- SEM. *P < 0.05, **P < 0.01, ***P < 0.001, ****P < 0.0001, unpaired t test. APF, alpha fetoprotein; EB, embryoid body; FOXOA2, forkhead box A2; MYH, myosin heavy chain; NKX2.5, NK2 homeobox 5; TUBB3, tubulin beta 3 class III, WT, wild-type.

7

Figure S2. Characterization of RAF1^{S257L} iPSC line 2 (isRASb1.17) from second patient. Human iPSC-RAF1^{S257L} line 2 reveals expression of pluripotency markers, a normal karyotype, and differentiation potency towards ectodermal, endodermal and mesodermal derivatives *in vitro*.

A) iPSCs-RAF1^{S257L} line 2 stain positive for OCT4, NANOG, SSEA3 and SSEA4 as detected by immunofluorescence staining. Scale bar, 200 µm.

B) RT-PCR analysis of pluripotency markers in iPSCs and control fibroblasts.

C) Flow cytometry analysis confirmed more than 99% of iPSCs stain positive for OCT4 and TRA-1-60.

D) Sanger sequencing confirmed the heterozygous RAF1^{S257L} variant in iPSCs (asterisk).

E) iPSCs show a normal diploid karyotype.

F, G) Trilineage differentiation of iPSC-RAF1^{S257L}. Expression of endodermal (SOX17 and FOX2A), mesodermal (*α-SMA*, *HAND1*, NKX2.5, and sarcomeric alpha-actinin) and ectodermal (TUBB3 and *PAX7*), markers were detected by RT-PCR and immunofluorescence staining. Scale bar, 200 µm.

H) CRISPR-CAS9 mediated correction of the RAF1^{S257L} mutation to RAF1^{WT} for the line 2 iPSCs (isRASb1-corr.9).
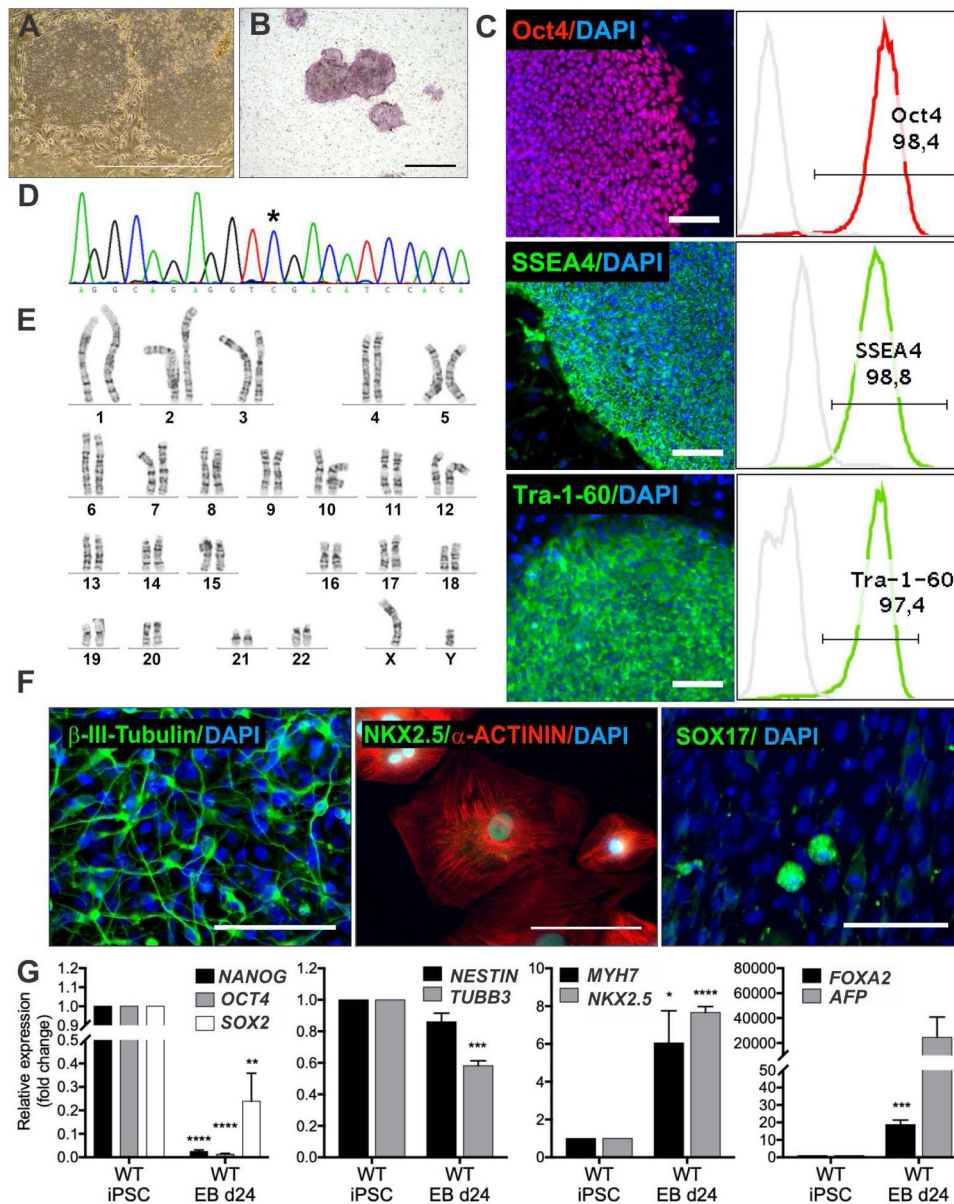
Figure S3. Characterization of WT iPSC line ipWT16.1 from donor 1 (WT1)

A) Typical iPSC colonies on mitotically inactivated murine feeder cells. Scale bar, 1000 μm.

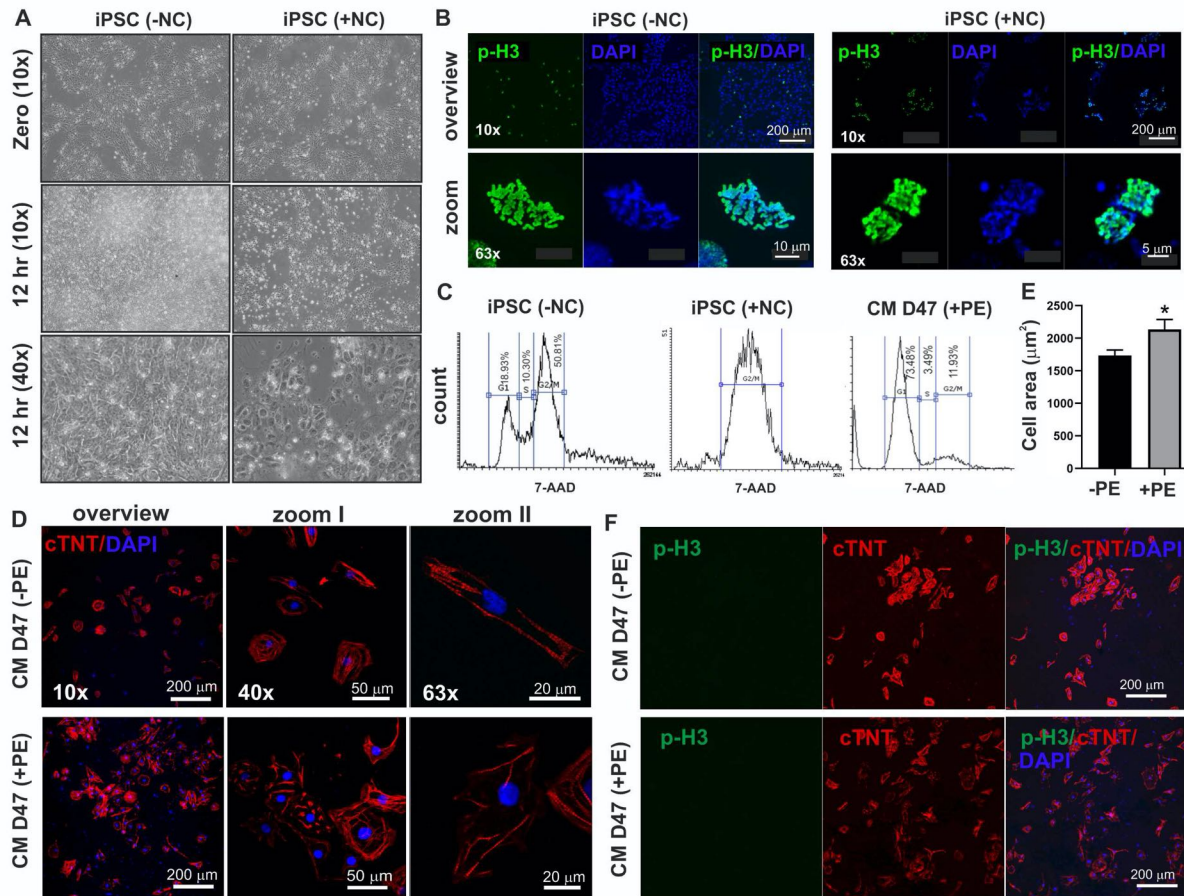B) Alkaline phosphatase-positive colonies. Scale bar, 1000 μm.

C) Expression of pluripotency markers OCT4, SSEA4, and TRA-1-60 as detected by immunofluorescence staining and flow cytometry. Scale bar, 100 μm. Isotype controls of flow cytometry histograms depicted in light gray.

D) Sanger sequencing confirmed the wildtype RAF1 sequence in iPSCs (asterisk).

E) Normal diploid karyotypes in iPSCs at passage 8 after reprogramming.

F) Trilineage differentiation of patient derived iPSCs. Expression of ectodermal (beta-III-Tubulin), mesodermal (NKX2.5 and sarcomeric alpha-actinin), and endodermal (SOX17) markers was detected. Scale bars, 100 μm.

G) Relative gene expression of pluripotency (*NANOG*, *OCT4*, *SOX2*) and differentiation markers (*NESTIN*, *TUBB3*, *MYH7*, *NKX2.5*, *FOXA2*, *AFP*) of differentiated embryoid bodies on d24 of differentiation relative to undifferentiated iPSCs normalized by beta-actin expression. Bar graphs represent mean of three independent samples +/- SEM. *P < 0.05, **P < 0.01, ***P < 0.001, ****P < 0.0001, unpaired t test. APF, alpha fetoprotein; EB, embryoid body; FOXOA2, forkhead box A2; MYH, myosin heavy chain; NKX2.5, NK2 homeobox 5; TUBB3, tubulin beta 3 class III, WT, wild-type.

Figure S4. Morphology of the RAF1^{S257L} iPSC line 1 after Nocodazole (NC) and phenylephrine (PE) treatments.

A) Illustration of cells arrested in mitosis upon NC treatment (100 nM) (lower panels).

B) phospho-histone 3 (p-H3) standing of human iPSC with different magnifications after NC treatment.

C) Cell cycle analysis of iPSC untreated and treated with NC as well as CMs treated with (PE).

D, E) cTNT staining of the dissociated CM showed increase in cell size of the CM treated with 100 nM of PE for 7-days. Confocal images of CMs treated with +PE were analyzed to determine the cell area using ImageJ software. Eighty-seven cells for the CTRL (-PE) and 59 cells for PE treatment were analyzed. The mean cell area is depicted and the SEM. Bar graphs represent mean of at least three independent samples +/- SEM. *P < 0.05, unpaired t test.

F) p-H3 staining of untreated (-PE) and PE-treated CM (+PE).

CM, cardiomyocytes; cTNT, cardiac troponin T; iPSC, induced pluripotent stem cells; PE, phenylephrine; p-H3, phospho-histone 3; NC, Nocodazole.
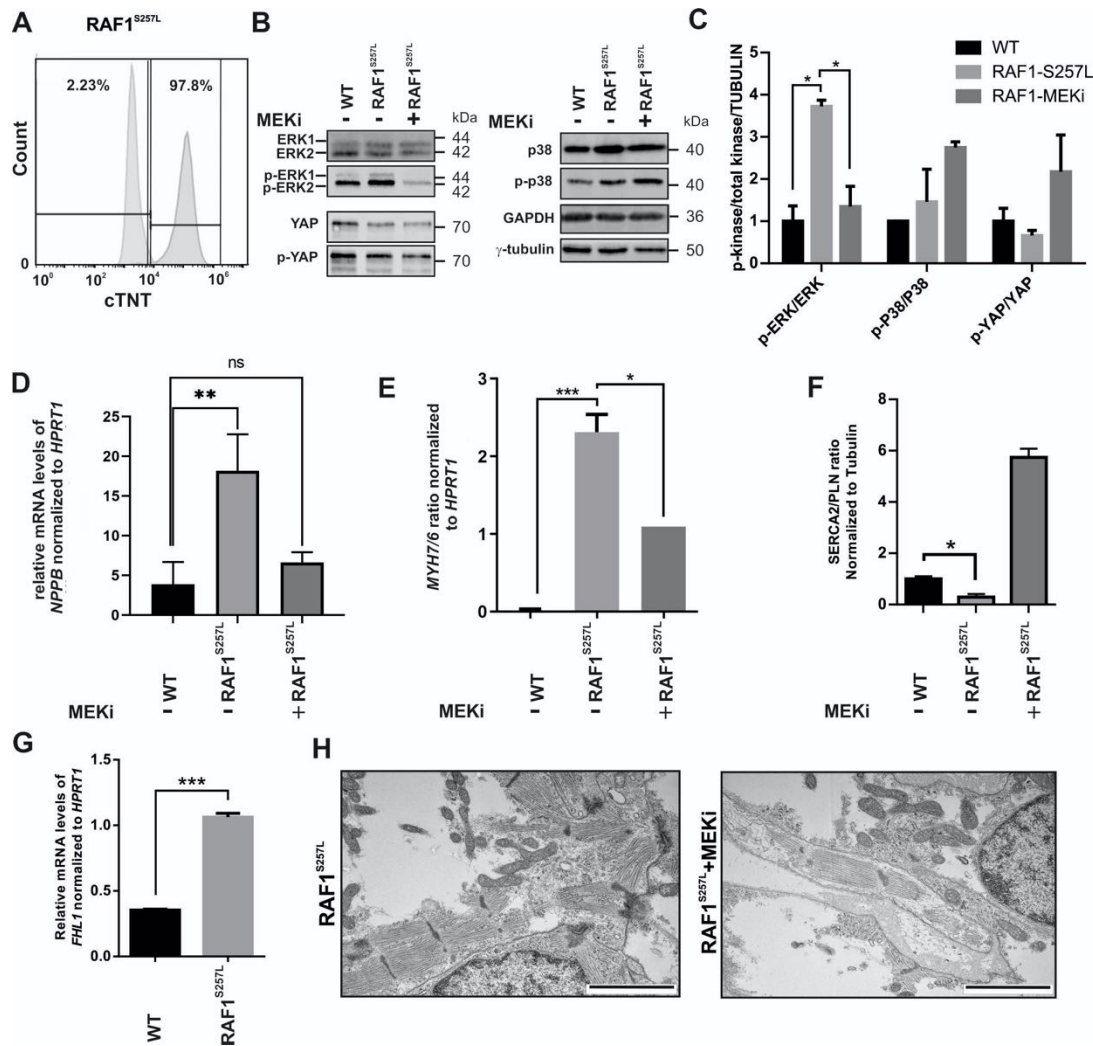
Figure S5. Cardiac myocyte generation and analysis from second individual that carries RAF1^{S257L}.

A) Expression of cardiac troponin C marker by flow cytometry at day 24 of cardiac differentiation.

B) Western blots analysis of the mentioned signaling molecules, p-ERK/ERK, p-YAP/YAP, and p-p38/p38.

C) Quantification of phospho-protein to total protein ratios. *P < 0.05, unpaired 1-tail t-test, n≤2.

D) Quantitative real-time PCR analysis of *NPPB* transcript levels. **P < 0.01, unpaired 2-tail t-test, n≤2.

E) *MYH7-to-MYH6* ratio was compared between WT CBs and RAF1^{S257L} CBs according to $2^{(-\Delta ct)}$ values.

F) Quantification of western blot results of SERCA2/PLN protein ratio normalized to Tubulin. *P < 0.05, unpaired 2-tail t-test, n≤2.

G) Quantitative real-time PCR analysis of *FHL1* transcript levels, n≤2, technical replicates.

H) Electron microscopic images of RAF1 mutated CBs treated with 0.2 μM MEK inhibitor from d12 of differentiation, scale bar, 2 μm.
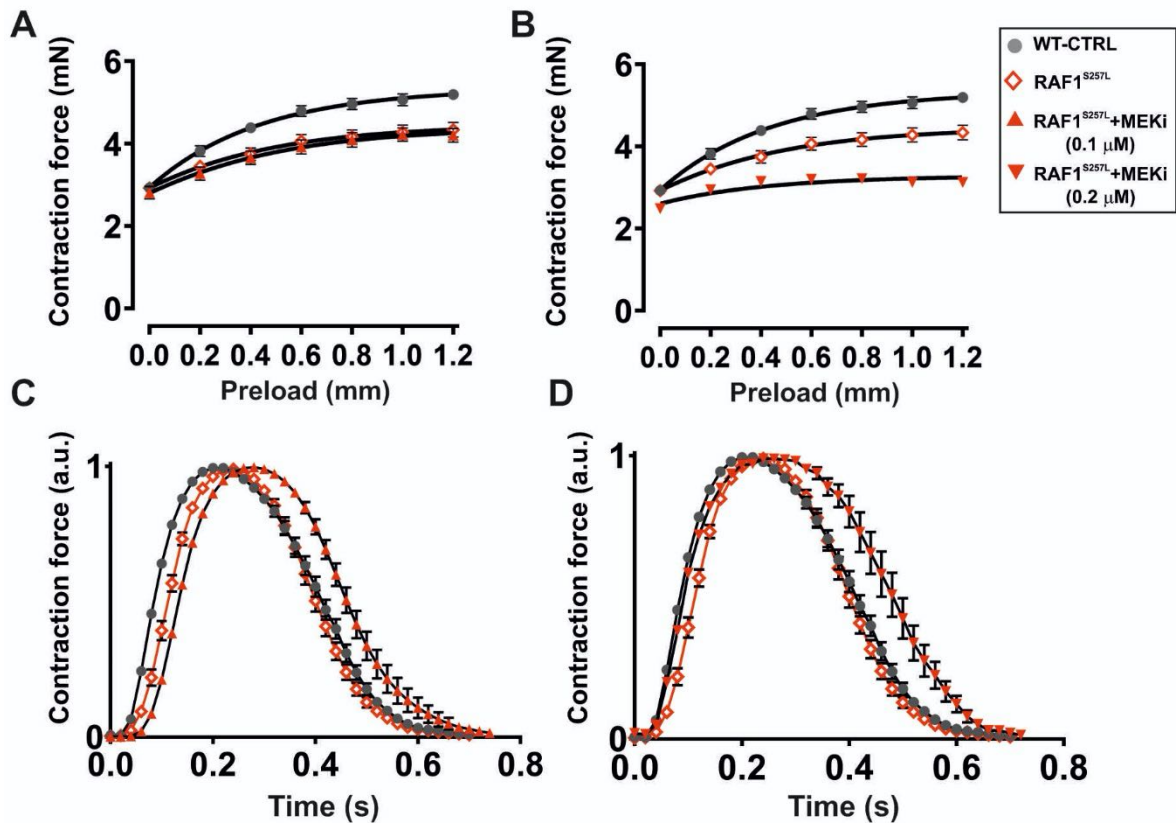
Figure S6. Effect of MEKi on the force development of human iPSC-derived bioartificial cardiac tissue.
A) Frank-Starling mechanism of: WT + RAF1 w/o + RAF w/ 0.1 µM MEKi.
B) Frank-Starling mechanism of: WT + RAF1 w/o + RAF w/ 0.2 µM MEKi.
C) Normalized contraction of: WT + RAF1 w/o + RAF w/ 0.1 µM MEKi.
D) Normalized contraction of: WT + RAF1 w/o + RAF w/ 0.2 µM MEKi.